Available online at www.eccomasproceedia.org
Eccomas Proceedia COMPDYN (2025) 667-681

ECCOMAS
Proceedia

COMPDYN 2025
10th ECCOMAS Thematic Conference on
Computational Methods in Structural Dynamics and Earthquake Engineering
M. Papadrakakis, M. Fragiadakis (eds.)
Rhodes Island, Greece, 15-18 June 2025

VULNERABILITY OF MASONRY STRUCTURES UNDER A COMBINATION OF LOADS DUE TO TSUNAMI AND EARTHQUAKE

A. Amato[1], L. Cavaleri[1], and M. C. Oddo[1]

[1] University of Palermo
Viale delle Scienze, Ed. 8, Palermo, 90128, Italy
e-mail: {anthea.amato, liborio.cavaleri, mariaconcetta.oddo01}@unipa.it

Abstract

Tsunamis are among the most catastrophic natural events, characterized by a low probability of occurrence but severe social and economic consequences, including high casualty rates and widespread destruction. Recent events have heightened awareness within the scientific community, revealing that approximately 60% of the coastal cities in the world —including those along the Mediterranean coasts — are at risk of tsunamis. Despite historical records, research on tsunami vulnerability in the Mediterranean regions remains limited due to insufficient hazard data and poor data quality.

This study investigates the vulnerability of masonry buildings typical of the Mediterranean coastline to tsunami impacts. Given that tsunamis frequently follow earthquakes, a probabilistic multi-hazard fragility assessment framework is introduced to analyze the cascading and compounding effects of earthquake-induced damage on structural performance under subsequent tsunami loading. A Monte Carlo based framework is adopted to account for uncertainties in tsunami loading and structural geometry ensuring a comprehensive vulnerability assessment. The study considers various earthquake intensities and tsunami scenarios to capture a wide range of possible multi-hazard conditions. The statistical results in terms of fragility curves demonstrate that structures become significantly more vulnerable when earthquake and tsunami hazards are considered together, as compared to assessing tsunami impact alone.

Keywords: tsunami, tsunami fragility, masonry, multi-hazard, tsunami vulnerability, Monte Carlo simulation.

ISSN:2623-3347 Published by Eccomas Proceedia.
Peer-review under responsibility of the organizing committee of COMPDYN 2025.
doi: 10.7712/120125.12438.25629

1 INTRODUCTION

In recent years, the assessment of tsunami vulnerability in coastal buildings has garnered significant attention, particularly following the major disasters occurred between the 2004 (Indian Ocen Tsunami [1]) and 2018 (Sulawesi Tsunami [2]). These catastrophic events have underscored the urgent need for comprehensive vulnerability studies to enhance the resilience of coastal structures and mitigate future risks.

The United Nations estimates that 60% of global coastal cities are at risk of tsunamis [3], including the Mediterranean coasts. Although they are less frequent and generally less severe compared to regions like the Pacific Ocean, the Mediterranean has experienced significant tsunami events. The most notable recent event is the 1908 Messina tsunami [4], triggered by a powerful earthquake with magnitude 7 that devastated the southern Italy. In fact, this dual catastrophe almost completely destroyed Messina, Reggio di Calabria, and numerous nearby coastal towns [5], causing an estimated 40,000 casualties.

The analysis of damage data from past tsunami events underscores the importance of studying the impact of tsunami forces on buildings and infrastructure to enhance risk management and develop effective mitigation strategies. Among the structures most vulnerable to tsunamis, masonry buildings have proven to be the most critical [6]. Given their widespread presence in the Mediterranean region [7], understanding the capacity of masonry structural components under tsunami loads is essential for deriving accurate fragility curves.

In recent years, several studies have focused on assessing the performance of masonry buildings under tsunami hazards [8-10]. Many of these studies rely on the development of empirical fragility curves based on field surveys and the visual analysis of high-resolution imagery of the considered areas. However, fewer studies have been addressed to developing analytical fragility curves, with most relying on simplified models that often not consider for prior earthquake damages [11-13]. Tsunamis frequently follow other natural events, particularly earthquakes. According to a global review, approximately 80% of tsunamis worldwide are triggered by seismic activity, with this percentage reaching 67% only in the Mediterranean region [14]. Often, along these coasts, existing masonry buildings were not designed for seismic resistance. As a result, earthquake damage can substantially compromise their structural integrity, making them more susceptible to subsequent tsunami forces. In this context, assessing the fragility of structures under multi-hazard scenarios (earthquake-tsunami) results crucial for evaluating the vulnerability of the Mediterranean coasts to tsunami risk. However, few studies have focused on the fragility assessment of buildings exposed to the combined effects of earthquakes and tsunamis. Most of the existing research has either addressed infrastructure [15, 16] or relied on overly simplified models [17]. Nevertheless, more advanced methodologies have also been explored. Particularly, Rossetto et al. [18] compared various dynamic and static approaches to analyze the response of a benchmark ten-storey reinforced concrete building subjected to sequential earthquake and tsunami events. Similarly, Attary et al. [19] proposed a methodology based on successive nonlinear analyses to develop fragility functions for a benchmark three-storey steel moment frame building under earthquake-tsunami loading. This approach also accounted for material uncertainties by employing Latin Hypercube Sampling, with each sample having a yield strength selected from 100 randomly generated values.

In this study, the methodology proposed by Xu et al. [15] and Attary et al. [19] for deriving fragility curves - originally applied to a benchmark steel frame structure and a four-span RC box-girder bridge, respectively, through successive nonlinear analyses under earthquake-tsunami sequences - was adopted and extended to masonry structures. Specifically, a probabilistic framework based on Monte Carlo simulations was developed to assess the numerical

and analytical multi-hazard fragility of various masonry structures, representative of typical geometrical and mechanical characteristics found in the Mediterranean regions, subjected to sequential earthquake-tsunami actions.

2 PROPOSED APPROACH FOR MULTI-HAZARD FRAGILITY ANALYSIS

The proposed probabilistic framework for developing multi-hazard fragility curves is based on the Monte Carlo simulation approach and adopts a two-stage damage methodology. This approach involves generating a set of randomly defined structural models and subjecting each to two sequential analyses. First, a nonlinear Time History Analysis (THA) is performed to simulate the effects of seismic loading. The resulting damaged structural state from the earthquake serves as the initial condition for the second analysis, i.e. a force-controlled Push-Over Analysis (POA), which simulates the effects of tsunami loading. This sequential analysis framework captures the degradation in structural capacity caused by the earthquake, providing a more realistic assessment of vulnerability under combined earthquake-tsunami scenarios. To optimize the computational efficiency, the entire process was implemented in Python [20], utilizing OpenSeesPy [21], a Python-based interface for the open-source Finite Element (FE) platform OpenSees, for structural analysis.

As illustrated in Figure 1, the procedure begins by assigning random geometric properties to each model. The structural response is first evaluated through THA under earthquake excitation, which serves as the initial structural condition for the subsequent tsunami analysis. The THA is performed using a spectrum compatible accelerogram, representing the ground motion characteristics of the earthquake. If the structural model collapses due to the seismic force, the procedure restarts by generating a new random structural model with different geometric characteristics, followed by another THA. Otherwise, if the structure withstands the earthquake but incurs damages, it is subsequently exposed to tsunami loading. In this phase, a Push-Over Analysis (POA) on the damaged model is conducted, where the tsunami loads are defined by random pairs of inundation depth (h) and flow velocity (v). Each time the structural model collapses due to tsunami forces, the corresponding inundation depth (h) at the point of failure is recorded in a count vector. At the end of the Monte Carlo simulations, the collected data are analyzed for obtaining the multi-hard fragility points, and the mean (μ) and standard deviation (β) of the logarithm of h are calculated as detailed in Oddo et al. [22]. These statistical parameters (μ and β) are then used to derive and plot the analytical fragility functions, which describe the probability of collapse exceedance under varying tsunami conditions.

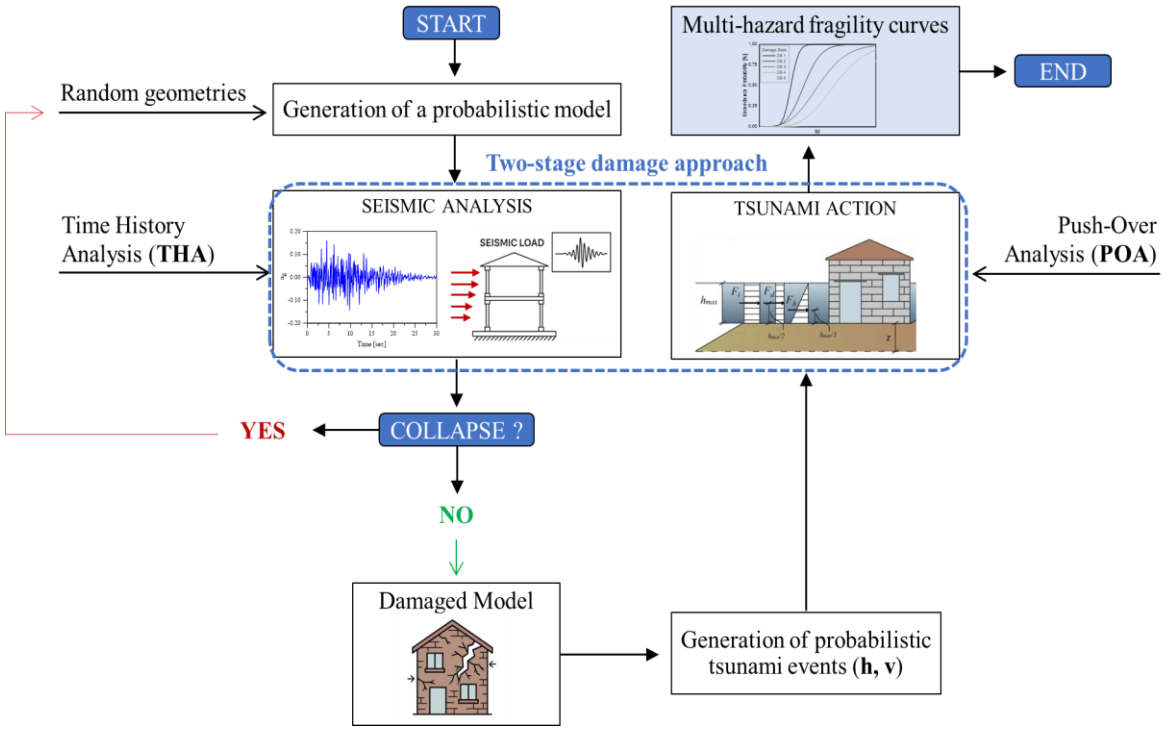

Figure 1: Framework for constructing multi-hazard fragility curves.

2.1 Structural modelling

Monte Carlo simulations were carried out on three groups of simplified limestone masonry structures representative of typical buildings found in Mediterranean regions [7]. These groups included one-, two-, and three-storeys configurations, as shown in Figure 2a, 2b and 2c, respectively.

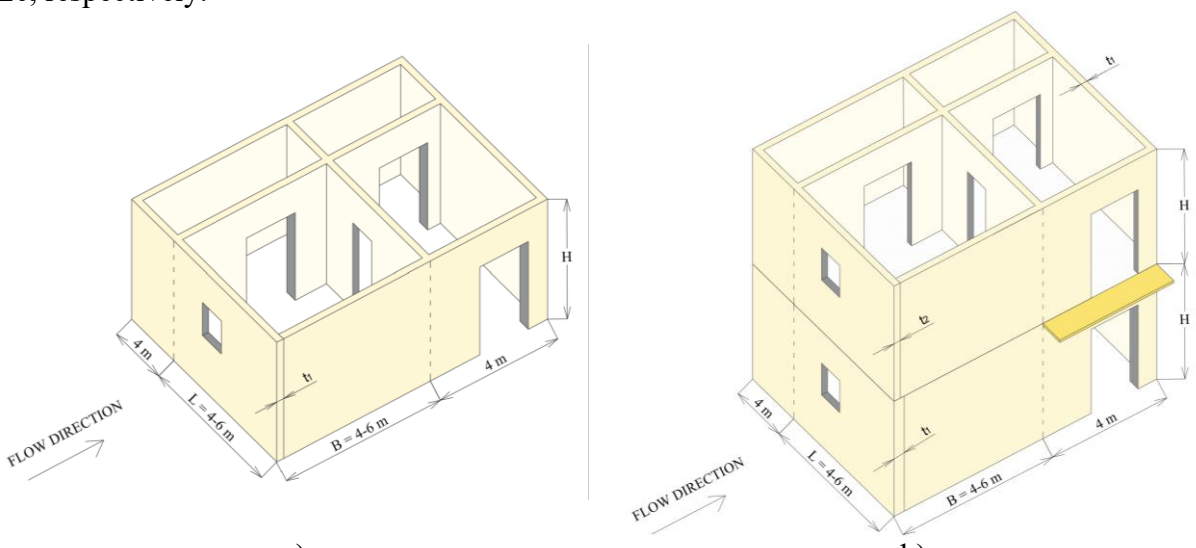

a) b)

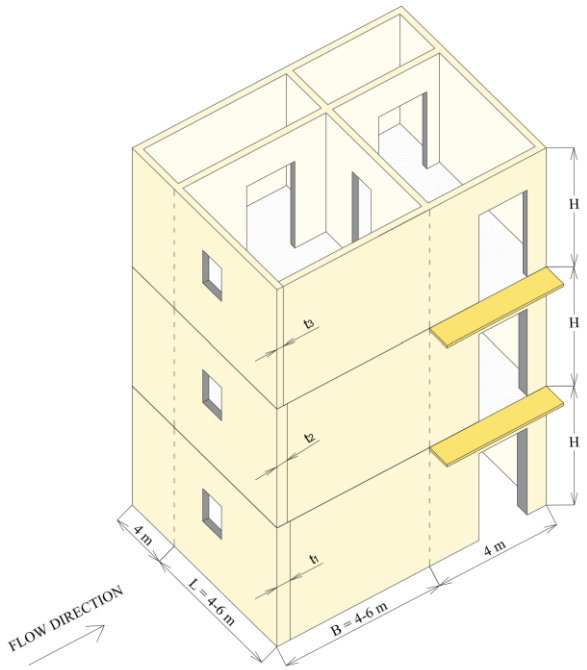

c)

Figure 2: General layout for three configurations of masonry buildings considered in this study: a) one-storey; b) two-storeys; c) three-storeys.

To incorporate the uncertainties inherent in the structural geometry, ten distinct structural models were generated for each group (one-storey, two-storeys and three-storeys) using randomly assigned geometric parameters. The randomized variables included: the length (L) of the masonry wall perpendicular to the tsunami flow direction, the length (B) of the masonry wall parallel to the tsunami flow direction, the wall thickness (t_1) at the first storey, and the wall height (H), as shown in Figure 2. Each variable followed a uniform probability distribution within the ranges specified in Table 1.

	Random Variable	Distribution	Range
Geometric variables	L	Uniform	4-6 m
	B		4-6 m
	t_1		0.4-0.9 m
	H		3-4 m

Table 1: Assigned distributions for geometric variables used in the simulation.

Moreover, to account for the reduction in wall thickness (t_i) in buildings with more than two storeys (i > 2), the following relationship was adopted:

$$t_i = t_1 - 0.1 \cdot (i - 1) \qquad \text{for i} > 2 \tag{1}$$

The structural response of each group of masonry buildings was analyzed using a capacity model that represents global collapse mechanisms consistent with the local failure modes of masonry walls. In this study, only the ground-floor masonry walls were considered, they were modeled as fiber-section beam elements of a simplified equivalent frame model [23].

In particular, each wall is modelled by two nonlinear beam-column elements (I and II) connected by a central node, where the mass (m) is concentrated. As schematized in Figure 3, the wall is assumed to be fixed at the base, while the top is free to rotate and translate along the y-direction. These simplified boundary conditions were adopted as they are commonly used for modeling masonry walls in existing buildings. However, despite these simplifications, the proposed modeling framework offers significant flexibility, allowing for the implementation of various constraint types.

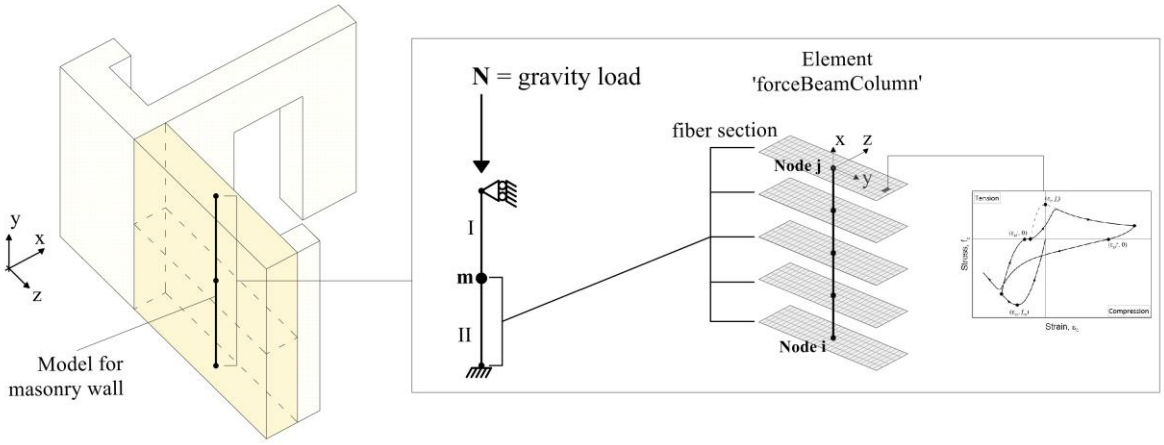

Figure 3: Fiber-section based model for masonry wall.

As shown in Figure 3, a uniaxial hysteretic constitutive model is adopted for the masonry fiber sections. Originally developed by Chang and Mander (1994) for concrete [24], this model is used here to simulate the hysteretic behavior of masonry under both cyclic compression and tension. The main parameters defining the shape of the envelope curve in both compression and tension are summarized in Table 2. These are based on an average compressive strength of f_m = 3.4 MPa, which reflects the typical mechanical properties of the most common masonry typologies in the Mediterranean region [7].

	f_m [MPa]	ε_{cc} [-]	E_c [MPa]	f_t [MPa]	ε_t [-]
Parameters	3.4	0.0025	1120	0.18	0.0002

Table 2: Parameters assumed for Chang and Mander uniaxial hysteretic constitutive model.

2.2 Tsunami modelling

The accuracy of tsunami models depends on their capability to replicate the forces observed during historical tsunami events, ensuring realistic representation of the loads acting on structures in the hazard area under study. Currently, there are few standards and guidelines, such as FEMA P-646 [25] and ASCE 7 [26], that provide recommendations for addressing tsunami-induced loads. According to ASCE/SEI 7-16 [26], tsunami effects on structures include a set of forces as shown in Figure 4: hydrostatic (F_h), buoyant, hydrodynamic (F_d), impulsive (F_i), debris impact, debris damming, uplift forces, and additional gravity loads resulting from retained water on elevated floors.

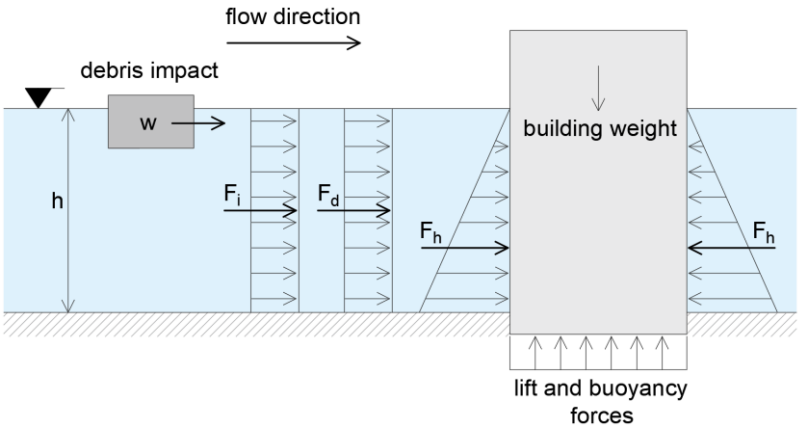

Figure 4: Fiber-section based model for masonry wall.

To simplify the analysis, in this study the analytical fragility curves are generated focusing primarily on the effects of hydrodynamic (F_d) and hydrostatic (F_h) forces according to the following Equations (2) and (3), respectively:

$$F_d = \frac{1}{2} \cdot \rho \cdot L \cdot C_D \cdot (h \cdot v^2) \tag{2}$$

$$F_h = \frac{1}{2} \cdot \rho \cdot g \cdot L \cdot h^2 \tag{3}$$

where ρ is the fluid density including the sediments (1100 kg/m^3), g is the gravitational acceleration, L is the width of the wall surface impacted by the flow, and C_D is the drag coefficient assumed equal to 1.1.

Uncertainties associated with tsunami actions were incorporated into the analysis by generating random values of flow velocity (v) coupled to each inundation depth (h). Specifically, the inundation depths ranged from 0.5 m to 5.0 m in increments of 0.25 m for one-storey buildings, from 0.5 m to 7.0 m in increments of 0.50 m for two-storey buildings, and from 0.5 m to 9.0 m in increments of 0.50 m for three-storey buildings. For each value of inundation depth, 10 random flow velocity values were generated and associated, as shown in Figure 5, assuming a uniform probability distribution. These velocity values were sampled within the range of 0.1 m/s to a maximum velocity v_{max}, which was calculated based on the Froude number (F_r), ideally not exceeding 2. Accordingly, v_{max} was calculated as:

$$v_{max} = F_r \cdot \sqrt{g \cdot h} \tag{4}$$

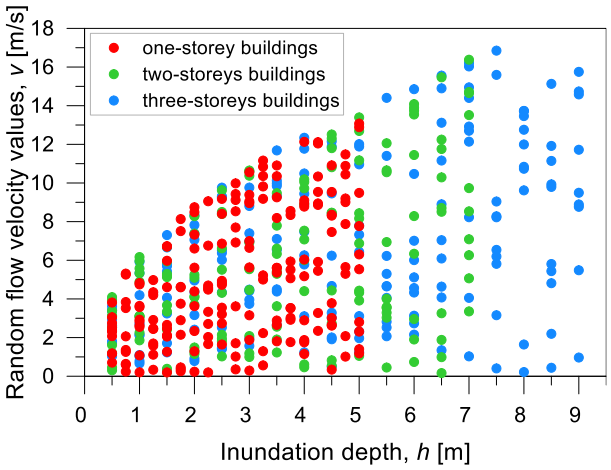

Figure 5: Random flow velocity values vs inundation depths.

2.3 Two-stage damage approach

A two-stage damage approach is adopted to analyze the response of masonry buildings subjected to sequential earthquake-tsunami loading. As illustrated in Figure 1, each structural model is first subjected to dynamic loading through a nonlinear time-history analysis and then to tsunami loading through a push-over analysis.

A spectrum-compatible accelerogram is applied in the horizontal x-direction to simulate ground motion through a transient dynamic analysis. The structural response, in terms of shear versus displacement for a benchmark model, is illustrated in Figure 6. In the present study, three levels of seismic intensity are considered, corresponding to Peak Ground Acceleration (PGA) values of 0.15g, 0.25g, and 0.50g.

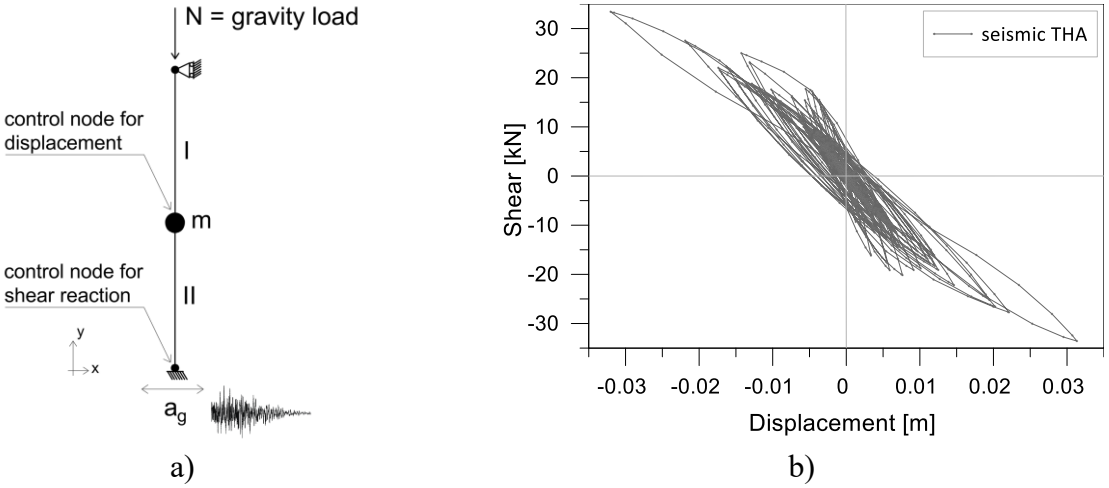

Figure 6: Dynamic loading through a nonlinear time-history analysis: a) structural model with no damage; b) shear-displacement curve obtained from seismic THA.

At the end of the dynamic analysis, the post-earthquake damage state of the masonry wall is kept and used as the initial condition for the second stage of the simulation (Figure 7a). In this second phase, a force-controlled POA is performed to simulate the effects of tsunami loading, following the scheme in Figure 7a. The resulting structural response, in terms of shear versus displacement, is presented in Figure 7b.

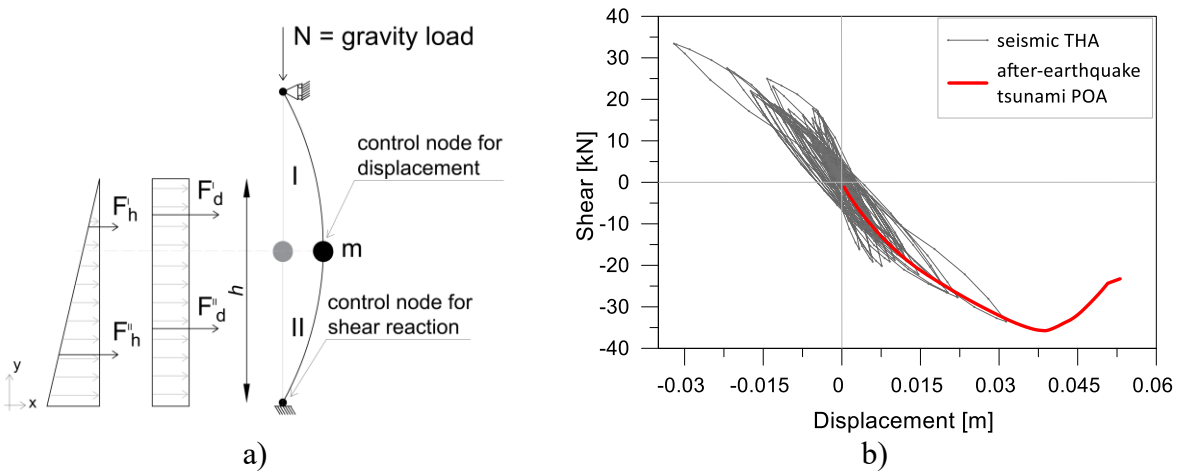

Figure 7: Tsunami loading through a force-controlled push-over analysis: a) post-earthquake-damaged structural model; b) shear-displacement curve obtained from seismic THA and post-earthquake tsunami POA.

This approach allows for the evaluation of the residual structural capacity of a building already damaged by an earthquake when subjected to subsequent tsunami forces, thereby capturing the cumulative effects of sequential earthquake–tsunami hazards.

Comparing the structural response in terms of shear–displacement curves for a masonry wall under tsunami loading, both with and without prior earthquake damage (red and green curves of Figure 8, respectively), it is evident that the damaged model exhibits a reduction in both stiffness and maximum load-carrying capacity.

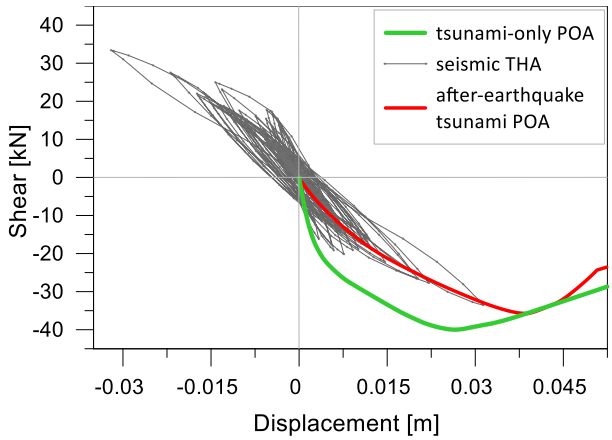

Figure 8: Comparison of numerical responses: tsunami-only POA (green curve), seismic THA (gray cyclic curve), and tsunami POA following earthquake damage (red curve).

3 FRAGILITY CURVES CONSTRUCTION

Based on the Monte Carlo simulations, according to the procedure described in the previous section, numerical fragility data points were obtained for each building typology (one-, two- and three-storeys buildings) and for different levels of earthquake intensity (no earthquake, PGA=0.15g, PGA=0.25g, and PGA=0.50g).

Specifically, for each simulation where structural failure occurred, either due to the seismic action or the subsequent tsunami, the information was recorded. When failure was attributed

to tsunami loading, the corresponding inundation depth (h) was stored into a count vector, as fragility curves are constructed with respect to the inundation depth as Intensity Measure (IM).

At the end of this procedure a dataset of statistical fragility points was obtained that enabled the numerical estimation of collapse probabilities at various inundation depths.

Assuming a lognormal analytical distribution $f(h)$, the mean μ and standard deviation β of the logarithms of inundation depths causing collapse are calculated, without excluding cases where collapse occurred due to the prior earthquake:

$$f(h) = \frac{1}{h\,\beta\,\sqrt{2\pi}} \exp\left(-\frac{(\ln h - \mu)^2}{2\beta^2}\right) \tag{5}$$

Then to account for the percentage of buildings that collapsed due to seismic action alone, the analytical probability density function *f(h)* is horizontally shifted by a value of $\bar{h}$, as shown in Figure 9, obtained by solving the following integral:

$$\int_0^{\bar{h}} f(h)dh \; = k \tag{6}$$

Here, k represents the percentage of buildings that collapsed due to the earthquake alone, and resulting from Monte Carlo simulations.

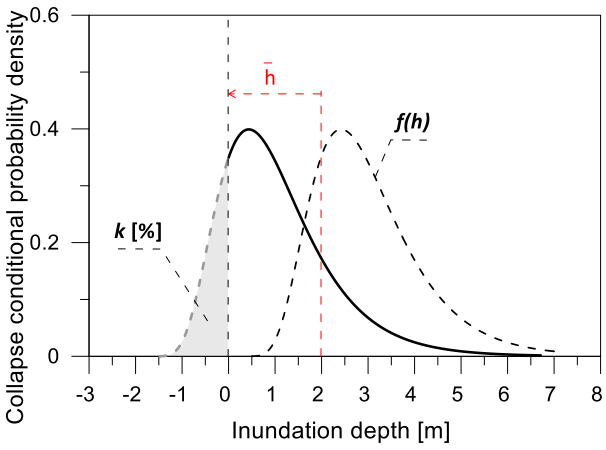

Figure 9: Shift of the conditional probability density function to account for earthquake-induced collapse.

Based on this, the final analytical fragility function is expressed through the lognormal cumulative distribution function *F(h)* as follows:

$$F(h) = k + (1 - k) \cdot \Phi\left(\frac{\ln h - \mu}{\beta}\right) \tag{7}$$

where Φ is the cumulative distribution function of the standard normal distribution.

4 RESULTS AND COMPARISONS

Combining the results obtained from the Monte Carlo simulations, according to the procedure detailed in the previous sections, for each group of masonry buildings, subjected to different levels of earthquake intensity and varying tsunami scenarios characterized by the inundation depth (used as the intensity measure, IM), both multi-hazard fragility curves and fragility surfaces were constructed.

Figure 10 shows the numerical fragility points obtained from Monte Carlo simulations alongside the corresponding analytical fragility curves for one-, two-, and three-storey masonry buildings, highlighting as the analytical fragility curves (solid lines), derived using the proposed adjustment procedure for the standard lognormal cumulative distribution function, are in good agreement with fragility points numerically obtained.

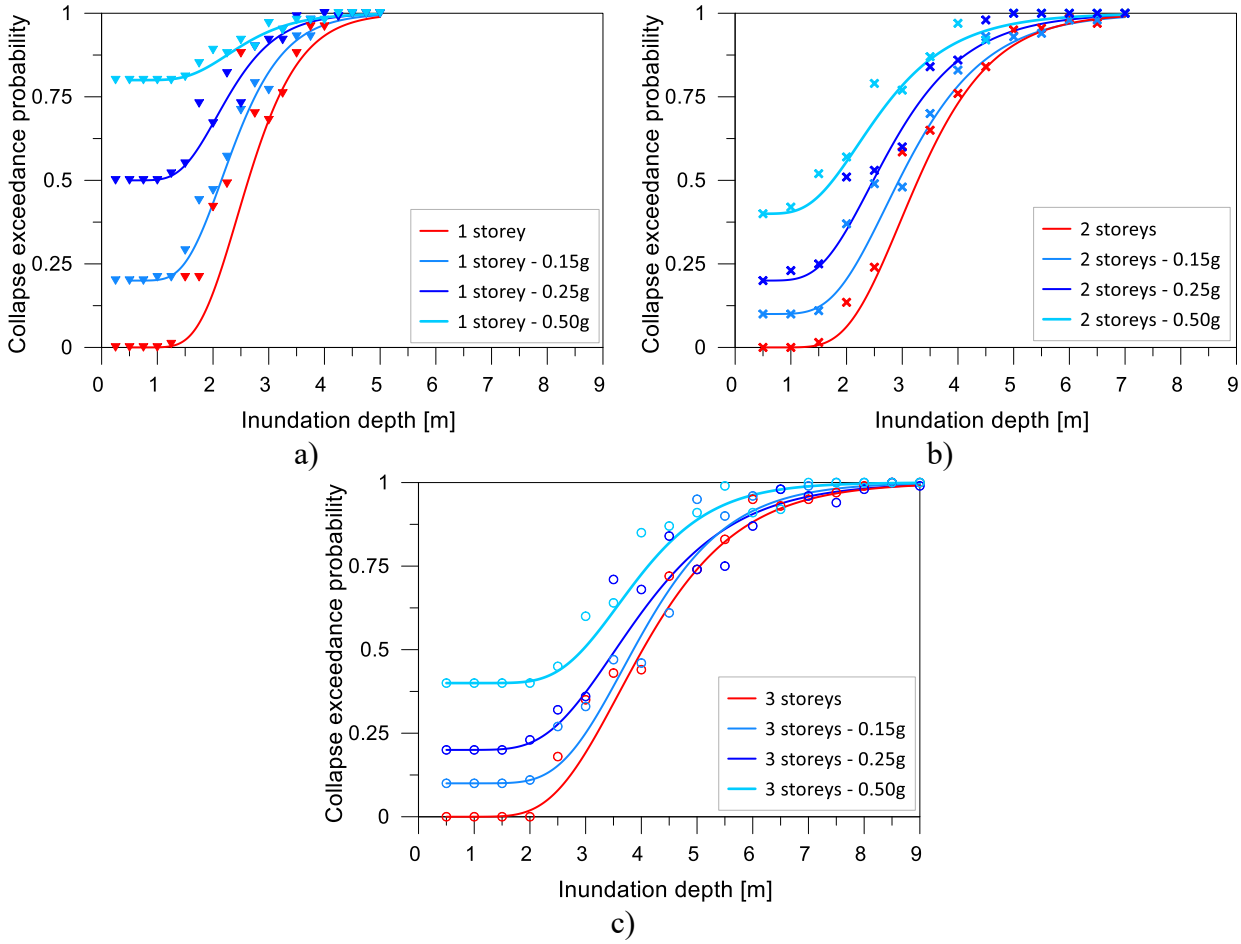

Figure 10: Comparisons of tsunami fragility curves for buildings damaged by various previous earthquake intensity levels: a) one-storey masonry buildings; b) two-storeys masonry buildings; c) three-storeys masonry buildings.

A key trend emerges when considering the impact of preceding earthquake damage: fragility curves exhibit a characteristic horizontal branch at low inundation depths, representing the probability of collapse due to seismic action before the tsunami actions. For example, at a PGA of 0.15g, the probability of collapse is already 20% for one-storey buildings (Figure 10a), and approximately 10% for two- and three-storeys buildings (Figures 10b and 10c). As seismic intensity increases to 0.25g and 0.50g, the percentage of structures collapses solely due to the earthquake rises, reaching 50% and 80% for one-storey buildings, and 20% and 40% for two- and three-storeys buildings, respectively.

Moreover, comparing the multi-hazard fragility curves across different seismic intensities reveals that the tsunami inundation height required to induce the structural failure decreases with increasing earthquake intensity. This relationship underscores the role of seismic predamage in weakening structures and accelerating collapse under subsequent tsunami loads. This effect is more pronounced in buildings with lower vertical loads. For one-storey build-

ings, the proportion of collapses due to seismic action increases nearly linearly with earthquake intensity, suggesting seismic forces dominate the failure mechanism. However, for two- and three-storeys buildings, where the vertical load is higher, the influence of the earthquake on collapse probability is less than proportional. In these cases, tsunami forces become more dominant, especially at greater inundation depths, where fragility curves for different seismic intensities converge. This behavior indicates that tsunami-induced failure in taller buildings becomes increasingly independent of prior seismic damage.

These findings are further presented in terms of multi-hazard fragility surfaces, in Figure 12. The surfaces capture the evolution of collapse probability as a function of both earthquake intensity (PGA) and tsunami inundation depth. They highlight the interplay between seismic pre-damage and tsunami loads, demonstrating how vulnerability shifts depending on structural height and loading conditions.

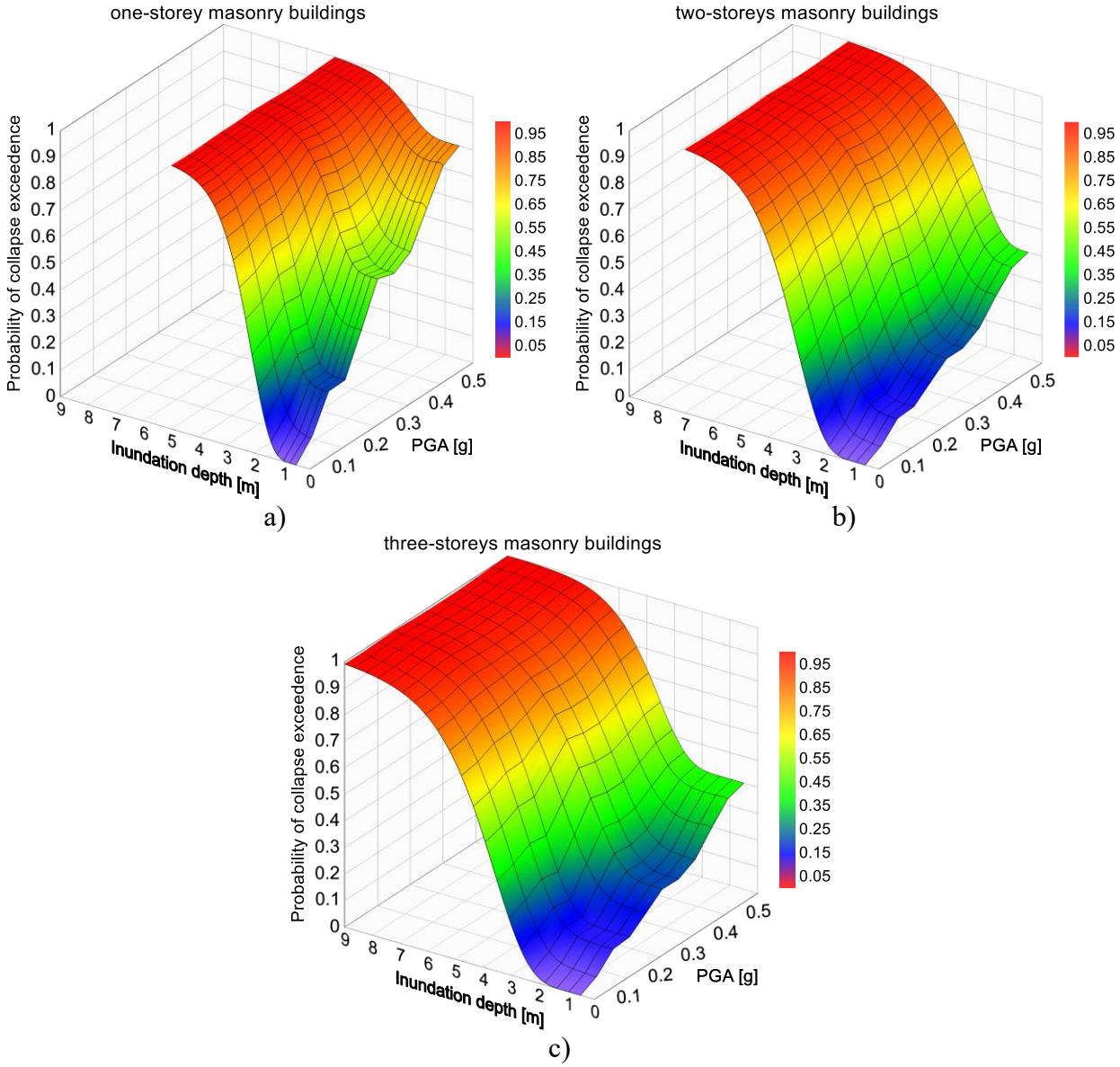

Figure 12: Post-shock PGA-dependent tsunami fragility surface: a) one-storey masonry buildings; b) two-storeys masonry buildings; c) three-storeys masonry buildings.

5 CONCLUSIONS

The present study proposes a simplified framework for developing multi-hazard fragility curves. The effectiveness of the procedure is evaluated by applying the proposed methodology to three groups of masonry buildings typical of the Mediterranean area, characterized by one-, two-, and three-storeys, due to the past tsunami events experienced preceding by earthquake actions. The results provide that:

- Earthquake damage in buildings, that do not collapse, induces a loss in terms of both maximum loads carrying capacity and stiffness.
- One-storey buildings are more vulnerable than two- and three-storeys buildings due to the vertical load is much lower and induce a weakness both for earthquake and tsunami loading.
- As expected, the increase of PGA induce damage in the structures that anticipate the collapse for tsunami loads for inundation depths smaller than the ones required in absence of earthquake
- Not considering the accumulated damage due to prior earthquake events can lead to a less vulnerable estimation if multi-hazard of earthquake-tsunami is not considered.

Beyond these results, the proposed methodology, based on Monte Carlo simulation and a simplified modeling strategy, offers a flexible framework for multi-hazard fragility assessment. It can be readily extended to other structural typologies, larger model populations, or enhanced with more sophisticated modeling and probabilistic inputs, depending on the objectives and scope of future investigations.

ACKNOWLEDGMENTS

This study was carried out within the PRIN 2022, cod. 2022YBAXTY_003, "MITICO - MItigation of Tsunami Impact on COstal regions", CUP B53D23006610006, and received funding from the European Union Next-Generation EU (National Recovery and Resilience Plan – NRRP, Mission 4, Component 2, Investment 1.1).

REFERENCES

[1] A. Ruangrassamee, H. Yanagisawa, P. Foytong, P. Lukkunaprasit, S. Koshimura, F. Imamura, Investigation of tsunami-induced damage and fragility of buildings in Thailand after the December 2004 Indian Ocean tsunami. *Earthquake Spectra*, 22(3_suppl), 377-401, 2006.

[2] T. Mikami, T. Shibayama, M. Esteban, T. Takabatake, R. Nakamura, Y. Nishida, ... K. Ohira, Field survey of the 2018 Sulawesi tsunami: Inundation and run-up heights and damage to coastal communities. *Pure and Applied Geophysics*, 176, 3291-3304, 2019.

[3] R. A. D. V. Rajapaksha, C. S. A. Siriwardana, A systematic review on different approaches used in the development of fragility curves for buildings. *12th International Conference on Structural Engineering and Construction Management*. Springer, Singapore, 2023.

[4] N. N. Ambraseys, Data for the investigation of the seismic sea-waves in the Eastern Mediterranean. *Bulletin of the seismological Society of America*, 52(4), 895-913, 1962.

[5] A. Billi, L. Minelli, B. Orecchio, D. Presti, Constraints to the cause of three historical tsunamis (1908, 1783, and 1693) in the Messina Straits region, Sicily, southern Italy. *Seismological Research Letters*, 81(6), 907-915, 2010.

[6] A. Suppasri, E. Mas, I. Charvet, R. Gunasekera, K. Imai, Y. Fukutani, F. Imamura, Building damage characteristics based on surveyed data and fragility curves of the 2011 Great East Japan tsunami. *Natural Hazards*, 66, 319-341, 2013.

[7] M. F. Ferrotto, L. Cavaleri, Masonry structures: A proposal of analytical generation of fragility functions for tsunami impact–Application to the Mediterranean coasts. *Engineering Structures*, 242, 112463, 2021.

[8] N. Valencia, A. Gardi, A. Gauraz, F. Leone, R. Guillande, New tsunami damage functions developed in the framework of SCHEMA project: application to European-Mediterranean coasts. *Natural Hazards and Earth System Sciences*, 11(10), 2835-2846, 2011.

[9] E. Mas, S. Koshimura, A. Suppasri, M. Matsuoka, M. Matsuyama, T. Yoshii, ... F. Imamura, Developing Tsunami fragility curves using remote sensing and survey data of the 2010 Chilean Tsunami in Dichato. *Natural Hazards and Earth System Sciences*, 12(8), 2689-2697, 2012.

[10] A. Suppasri, I. Charvet, K. Imai, F. Imamura, Fragility curves based on data from the 2011 Tohoku-oki tsunami in Ishinomaki city, with discussion of parameters influencing building damage. *Earthquake Spectra*, 31(2), 841-868, 2015.

[11] A. Ruangrassamee, H. Yanagisawa, P. Foytong, P. Lukkunaprasit, S. Koshimura, F. Imamura, Investigation of tsunami-induced damage and fragility of buildings in Thailand after the December 2004 Indian Ocean tsunami. *Earthquake Spectra*, 22(3_suppl), 377-401, 2006.

[12] K. I. U. Nanayakkara, W. P. S. Dias, Fragility curves for structures under tsunami loading. *Natural Hazards*, 80, 471-486, 2016.

[13] S. Belliazzi, G. P. Lignola, M. Di Ludovico, A. Prota, Preliminary tsunami analytical fragility functions proposal for Italian coastal residential masonry buildings. *In Structures*, Vol. 31, pp. 68-79, 2021.

[14] J. A. Reid, W. D. Mooney, Tsunami occurrence 1900–2020: A global review, with examples from Indonesia. *Pure and Applied Geophysics*, 180(5), 1549-1571, 2023.

[15] J. G. Xu, G. Wu, D. C. Feng, J. J. Fan, Probabilistic multi-hazard fragility analysis of RC bridges under earthquake-tsunami sequential events. *Engineering Structures*, 238, 112250, 2021.

[16] H. Mei, A. Guo, Seismic-tsunami fragility analysis for box-girder simple-support bridge with transverse RC constrainers. *Ocean Engineering*, 304, 117578, 2024.

[17] S. Park, J. W. Van de Lindt, D. Cox, R. Gupta, F. Aguiniga, Successive earthquake-tsunami analysis to develop collapse fragilities. *Journal of Earthquake Engineering*, 16(6), 851-863, 2012.

[18] T. Rossetto, C. De la Barra, C. Petrone, J. C. De la Llera, J. Vásquez, M. Baiguera, Comparative assessment of nonlinear static and dynamic methods for analysing build-

ing response under sequential earthquake and tsunami. *Earthquake Engineering & Structural Dynamics*, 48(8), 867-887, 2019.

[19] N. Attary, J. W. Van De Lindt, A. R. Barbosa, D. T. Cox, V. U. Unnikrishnan, Performance-based tsunami engineering for risk assessment of structures subjected to multi-hazards: tsunami following earthquake. *Journal of Earthquake Engineering*, 25(10), 2065-2084, 2021.

[20] F. McKenna, OpenSees: a framework for earthquake engineering simulation. *Computing in Science & Engineering*, 13(4), 58-66, 2011.

[21] M. Zhu, F. McKenna, M. H. Scott, OpenSeesPy: Python library for the OpenSees finite element framework. *SoftwareX*, 7, 6-11, 2018.

[22] M. C. Oddo, P. G. Asteris, L. Cavaleri, Monte Carlo analysis of masonry structures under tsunami action: reliability of lognormal fragility curves and overall uncertainty prediction. In *Structures*, Vol. 63, p. 106421, 2024.

[23] M. Peruch, E. Spacone, G. Camata, Nonlinear analysis of masonry structures using fiber‐section line elements. *Earthquake Engineering & Structural Dynamics*, 48(12), 1345-1364, 2019.

[24] G.A. Chang, J.B. Mander, Seismic energy based fatigue damage analysis of bridge columns: Part I-evaluation of seismic capacity. *National Center for Earthquake Engineering Research*, Buffalo, NY, p 222, 1994.

[25] FEMA, Guidelines for Design of Structures for Vertical Evacuation from Tsunamis. (FEMA P-646). *FEMA P-646 Publ*, 2012.

[26] ASCE/SEI 7-16 (American Society of Civil Engineers), Minimum Design Loads for Buildings and Other Structures, Reston, Virginia, 2017.